J. Comp. App. Res. Mech. Eng. Vol. 15. No. 1, pp. 63-74, 2025 *DOI: 10.22061/jcarme.2025.10582.2401*

SRTTU

Journal of Computational and Applied Research in Mechanical Engineering

jcarme.sru.ac.ir

JCARME

ISSN: 2228-7922

Research paper

A vibration-based fault diagnosis method for rolling bearings via optimized wavelet-SVM fusion

A. Haitao Zhang[a,*], B. Li Guan[a] and C. Long Chang[b]

[a] *College of Mechanical Engineering, Nanjing Vocational University of Industry Technology, Nanjing, 210023, China.*
[b]*Tsinghua Shenzhen International Graduate School, Tsinghua University, Shenzhen, 518055, China.*

Article info:

Article history:

Received: 10/01/2024
Revised: 18/09/2025
Accepted: 23/09/2025
Online: 28/09/2025

Keywords:

Statistical features,
Wavelet packet decomposition,
Gaussian kernel function,
Principal component analysis,
Prediction accuracy.

[*]Corresponding author:
2022101343@niit.edu.cn

Abstract

Rolling bearings are critical components of rotating machinery, and their health status directly affects the operational reliability of equipment. This paper proposes an optimized wavelet-SVM fault diagnosis method based on multi-source vibration signal fusion: Three-channel inputs are constructed by synchronously collecting vibration signals from the drive end and fan end, along with their differential signals; Wavelet packet decomposition is utilized to extract frequency-domain features such as unit node energy entropy and wavelet coefficient standard deviation, while dimensionless indicators independent of rotational speed (kurtosis factor/waveform factor/impulse factor) are introduced to enhance time-domain characterization; The fused features are input into an RBF-SVM classifier after dimensionality reduction via PCA (retaining 99% variance, reducing dimensions from 102 to 4). Experiments indicate that on the CWRU dataset, this method achieves 97.0% precision, 96.9% recall, and an F1-score of 96.9% (representing a 2.9% improvement over single-source input methods); Although there is a 2.4% absolute accuracy gap compared to deep learning solutions, it possesses significant edge advantages—memory usage is only 12KB and inference latency is 0.6ms—providing a high-precision, low-cost embedded solution for rotating machinery fault diagnosis.

1. Introduction

Rolling bearings are key rotating components in mechanical equipment, serving as indispensable parts in various types of rotating machinery, while also being a significant source of equipment failures. Statistics show that approximately 45-55% of failures in rotating machinery can be attributed to rolling bearing failures [1]. Therefore, effective fault diagnosis of bearings is a crucial measure for maintaining the normal operation of rotating machinery and reducing downtime [2].

Fault diagnosis methods for bearings are primarily divided into two categories, namely model-based methods and data-driven methods [3, 4]. Among them, model-based methods typically rely on precise fault mechanism models to represent the faults and phenomena of monitored components through mathematical

approaches. These methods require extensive prior knowledge, and constructing an accurate fault mechanism model capable of adapting to changes in operating environments and mechanical physical structures is extremely difficult. In contrast, data-driven methods do not require consideration of the fault mechanism. They can achieve fault diagnosis solely based on condition signals (such as vibration signals, generally shown in Fig. 1).

However, data-driven fault diagnosis methods also face several challenges, such as:

① Limitations of edge computing devices. In industrial scenarios, fault detection for rotating components like bearings still primarily relies on sensor + microcontroller hardware as the underlying support, with microcontrollers typically featuring a main frequency <200 MHz, SRAM < 256KB, and power consumption <100mW. Furthermore, the requirement for bearing fault detection inherently demands that the detection model possesses low-latency characteristics.

② Interference from the noise of surrounding equipment. In industrial settings, the collection of bearing vibration signals inevitably suffers from noise interference from other nearby equipment, necessitating that the employed method exhibits a certain level of noise immunity.

③ Limitations on model generalizability. Within industrial environments, bearings operate under varying rotational speeds, fault types, and loads, requiring the method used to possess sufficient generalization ability to adapt to as many operating conditions as possible.

To overcome the aforementioned shortcomings, this paper designs a lightweight fault diagnosis model based on multi-source vibration signals, with the main contributions as follows:

① Mitigating noise interference at the data level through data augmentation. The model inputs in this work are: the vibration signal from the fan end, the vibration signal from the drive end, and the difference between the vibration signals from the fan end and drive end. This approach significantly reduces the challenges posed by common-mode noise to model prediction.

Fig. 1. Sensor layout under actual operating conditions.

Additionally, during model training, 10dB white noise is randomly added to the original vibration signals to further enhance model robustness.

② Employing refined feature engineering to extract detailed characteristics of the vibration signals from both time and frequency domains while denoising. For time-domain features, in addition to commonly used metrics such as mean, variance, peak, maximum, and minimum values, dimensionless indicators independent of rotational speed are introduced, including kurtosis factor, crest factor, waveform factor, impulse factor, and clearance factor.

For frequency-domain features, statistics insensitive to sampling frequency are also adopted, such as wavelet coefficient mean, wavelet coefficient standard deviation, and unit node energy entropy.

③ Incorporating PCA for feature dimensionality reduction between feature extraction and classifier prediction to further reduce computational demands, enabling the model to be directly deployed on battery-powered edge devices. This paper utilizes a total of 10 time-domain statistical features and 3 frequency-domain statistical features. When employing a 3-level wavelet packet decomposition, the total number of features amounts to:

$3\times2^3\times3+3\times10=102$. To further reduce the computational load for the classifier, PCA dimensionality reduction is applied, reducing the 102-dimensional vector to 4 dimensions.

2. Related works

In recent years, deep learning-based intelligent fault diagnosis methods have been widely adopted in the field of mechanical fault diagnosis within academia due to their ability to

automatically learn features from data without requiring specialized expertise [5]. For instance, models such as GRU [6], LSTM [7], and Transformer [8] can adaptively capture features from time series and iteratively optimize model detection accuracy through gradient backpropagation via loss functions.

For example, Chen, *et al.* [9] utilized a Deep Graph Convolutional Network (DGCN) to classify compound faults in rolling bearings and achieved promising results. Wang, *et al.* [10] proposed a CNN-GRU network that leverages CNN to capture local features and GRU to capture global features of time series, thereby enabling fault classification.

However, these deep learning-based models face deployment challenges (requiring frameworks like TensorFlow Lite, and even after INT8 quantization, model size >500KB) and high computational complexity (single inference >100ms).

In contrast, the technical approach using traditional feature engineering combined with SVM remains valuable, reflected in: low memory footprint (model size <50KB), low computational complexity (single inference ~10ms), and low difficulty in edge deployment (implemented in pure C code, no dependency libraries required).

Recent research (2019~2025) adopting similar technical approaches includes: Li, *et al.* [11] integrated the concept of fusion stacked representation learning (S-RL) with Least Squares Support Vector Machine (LS-SVM) to propose the DSLS-SVM model. This model integrates multiple LS-SVM modules via a stacked structure. Experiments on the CWRU dataset demonstrated the model's good effectiveness and applicability. However, this method only considered time-domain features of vibration signals, neglecting frequency-domain features, making its predictions susceptible to time window size and sensor placement, potentially compromising robustness.

Shao, *et al.* [12] proposed an intelligent rolling bearing fault diagnosis method using Wavelet Packet Transform (WPT) to extract frequency-domain information and an Improved Particle Swarm Optimization (IPSO) algorithm to optimize SVM hyperparameter selection. Experiments showed the significant effectiveness of the proposed method. However, it did not account for noise interference and time-domain features under actual operating conditions, potentially limiting its generalization ability in real-world scenarios. Li, *et al.* [13] first employed WPT to extract frequency-domain information, then merged multi-scale wavelet coefficients into a one-dimensional vector. This feature vector was subsequently converted into a two-dimensional grayscale image, and finally, a Convolutional Neural Network (CNN) was constructed as the classifier for rolling bearing fault diagnosis.

However, this method requires a fixed image size as CNN input, making it difficult to adapt to different sampling frequencies. Sun, *et al.* [14] used EMD for vibration signal denoising, extracted features from the denoised signal using kurtosis and energy as statistics, and employed SVM as the classifier for fault diagnosis, achieving 99.3% recognition accuracy on the CWRU dataset.

However, this method neglected the frequency-domain characteristics of the signal. Wu, *et al.* [15] proposed an intelligent fault classification and diagnosis model for rolling bearings based on Fast Fourier Transform (FFT) and a temporal convolutional network with squeeze-and-excitation (SE-TCN) attention mechanism, using SVM as the classifier. FFT is applied within a time window to obtain current frequency-domain features, then SE-TCN iteratively extracts frequency-domain features for sliding time windows, followed by SVM for fault identification, achieving over 99% classification accuracy on the CWRU dataset.

However, this method did not consider sensor placement and noise interference, and the inclusion of TCN also imposes computational pressure on edge devices.

The method proposed in this paper achieves a better balance between detection accuracy, computational complexity, and robustness.

3. Methods

3.1. Pipeline overview

The method used in this paper is illustrated in Fig. 2. It takes as input the vibration signal from the fan end, the vibration signal from the drive end, and the difference between the fan end and drive

end vibration signals. Wavelet packet decomposition is employed to extract frequency-domain features. Threshold-based denoising is applied to denoise the three signals, which are then reconstructed back to the time domain.
Subsequently, time-domain statistical features are extracted from the denoised time-domain signals. The frequency-domain and time-domain features are then concatenated. This combined feature set undergoes dimensionality reduction via PCA (to reduce computational load for the classifier). Finally, fault classification is performed by an SVM.

3.2. Feature extraction in frequency domain based on wavelet packet decomposition

The wavelet transform has extensive applications in research fields such as signal analysis and image processing. It possesses the ability to highlight local features of signals in both the time and frequency domains. The formula for the discrete wavelet transform is shown in Eq. (1):

$$WT_f\left(a_0^j, k\tau_o\right) = \int f(t)\psi^*_{a_0^j, k\tau_o}(t)\,dt \tag{1}$$

In the equation, $WT_f\left(a_0^j, k\tau_o\right)$ represents the wavelet transform coefficient, where a_0^j denotes that at scale j, the sampling interval can be expanded by a factor of a_0^j. $f(t)$ represents the signal in the time domain, and $\psi^*_{a_0^j, k\tau_o}(t)$ represents the wavelet basis function corresponding to the specific scale and translation.

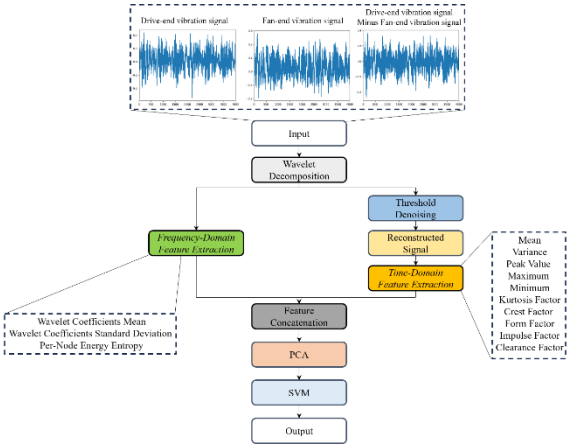

Fig. 1. Overall pipline.

Building upon this foundation, this paper selects wavelet coefficient mean, wavelet coefficient standard deviation, and per-node energy entropy as frequency-domain feature statistics. Their calculation formulas are as follows:
Wavelet coefficients mean:

$$\mu_j = \frac{1}{N_j}\sum_{k=1}^{N_j}\left|c_{j,k}\right| \tag{2}$$

In the formulas: j represents the decomposition level; N_j represents the total number of coefficients at level j; $c_{j,k}$ represents the wavelet coefficient at position k of level j.
Wavelet coefficients standard deviation [16]:

$$\sigma_i = \sqrt{\frac{1}{N_j - 1}\sum_{k=1}^{N_j}\left(\left|c_{j,k}\right| - \mu_j\right)^2} \tag{3}$$

Per-Node energy entropy [17]:

$$E_j = \frac{1}{N_j}\sum_{k=1}^{N_j}\left(c_{j,k}\right)^2 \tag{4}$$

3.3. Threshold method of small coefficients

It is a technique whose core involves processing each wavelet coefficient independently. The computational procedures for two representative methods—hard thresholding and soft thresholding—are as follows:
Hard threshold:

$$y = \begin{cases} x, & |x| > \lambda \\ 0, & |x| < \lambda \end{cases} \tag{5}$$

Soft threshold:

$$y = \begin{cases} sign(x)(|x| - \lambda), & |x| > \lambda \\ 0, & |x| < \lambda \end{cases} \tag{6}$$

After extracting the frequency-domain statistics of the vibration signal using wavelet packets, threshold denoising is applied to remove high-frequency noise from the signal, which is then reconstructed in the time domain.

3.4. Feature extraction in time domain based on statistical characteristic

Time-domain information represents the signal with the time axis as the abscissa, providing an

intuitive visualization of the vibration signal's waveform. Time-domain analysis aims to extract statistical features from the signal in the time domain, serving as a means to determine the operational state of the bearing. Given a time-domain signal $\{x_i\}, i = 1,2,\cdots,N$, the time-domain feature statistics used in this paper are:

Maximum:

$$ma = max(x(i)) \tag{7}$$

Minimum:

$$mi = min(x(i)) \tag{8}$$

Mean:

$$me = mean(x(i)) \tag{9}$$

Peak:

$$pk = ma - mi \tag{10}$$

Variance:

$$va = var(x(i)) \tag{11}$$

Waveform factor [18]:

$$S = rm/av \tag{12}$$

Peak factor:

$$C = pk/rm \tag{13}$$

Kurtosis factor [19]:

$$Kr = sum(x(i)^4)/\sqrt{sum(x(i)^2)} \tag{14}$$

Impulse factor [20]:

$$I = pk/av \tag{15}$$

Clearance factor [21]:

$$L = pk/xr \tag{16}$$

3.5 Feature dimensionality reduction based on principal component analysis.

For the three sets of vibration signals (fan end signal, drive end signal, and their differential signal), the combined time-frequency domain features total 102 dimensions. This includes 30 time-domain features (10 time-domain statistics per signal, with 3 input signals: 3 × 10 = 30) and 72 frequency-domain features (3 frequency-domain statistics per node, with a 3-level wavelet packet decomposition, where each signal has 2^3 nodes: 3 signals × 8 nodes × 3 statistics = 72).

To better adapt to industrial scenarios with low computational resources, this paper incorporates PCA for feature dimensionality reduction between feature extraction and classifier prediction. This further reduces computational demands, enabling the model to be directly deployed on battery-powered edge devices.

The specific process is described below.

Step 1: Input the feature matrix, denoted as X (where rows represent samples and columns represent features), and determine the cumulative contribution rate (set to 99% in this experiment).

Step 2: Transpose the feature matrix X and perform zero-mean normalization. Calculate the covariance matrix $D = \frac{1}{m}X^T X$.

Step 3: Solve for the eigenvalues λ and corresponding eigenvectors of the covariance matrix D.

Step 4: Calculate the contribution rate and cumulative contribution rate. Arrange the eigenvectors into a transformation matrix W in descending order of their corresponding eigenvalues. The expressions for the contribution rate and cumulative contribution rate are given by Eqs. (17 and 18), respectively.

$$a_i = \frac{\lambda_i}{\sum_{j=1}^{n}\lambda_j} \tag{17}$$

$$\beta_j = \frac{\sum_{i=1}^{k}\lambda_i}{\sum_{j=1}^{n}\lambda_j} \tag{18}$$

In Eqs. (17, 18), a_i represents the variance contribution rate of the i -th principal component, and β_j represents the cumulative

contribution rate of the j -th principal component.

3.6. Bearing fault classification based on support vector machine

The fundamental idea of SVM is to define the optimal linear hyperplane. The algorithm for finding this optimal hyperplane is formulated as a convex optimization problem. Furthermore, based on the Mercer kernel expansion, a nonlinear mapping φ projects the sample space into a high-dimensional or even infinite-dimensional feature space (Hilbert space), which is a generalization of Euclidean space. This enables the application of linear learning methods in the feature space to solve highly nonlinear classification and regression problems in the original sample space.
The mathematical model of the nonlinear SVM based on the kernel method is shown in Eq. (19):

$$\begin{aligned} &maxJ(\alpha) = \max\left(\sum_{i=1}^{l}\alpha_i - \right. \\ &\left.\frac{1}{2}\sum_{i=1,j=1}^{l}\alpha_i\alpha_j y_i y_j\left(\varphi(X_i)\cdot\varphi(X_j)\right)\right) \\ &s.t.\sum_{i=1}^{l}\alpha_i y_i = 0\ (C \geq \alpha_i \geq 0. i = 1.\cdots l) \end{aligned} \quad (19)$$

where l denotes the number of samples, $X_i \in R^l, y_i \in \{+1, -1\}, \alpha_i$ represents the lagrange multipliers, C is the penalty parameter, and $\varphi(X_i)$ represents the nonlinear transformation or mapping of X_i.
The optimal hyperplane decision function is finally derived as shown in Eq. (20):

$$M(X) = sgn(\sum_{\substack{Support\\ vectors}} a_i^* y_i\left(K(X,Y)\right) + b^*) \quad (20)$$

where K (X, Y) represents the Mercer kernel function, as shown in Eq. (21):

$$K(X,Y) = (\varphi(X_i)\cdot\varphi(X_j)) \quad (21)$$

4. Experiments and results

4.1. Dataset introduction and evaluation metrics

To validate the classification performance of the proposed method, the Case Western Reserve University (CWRU) bearing dataset [22] is used to evaluate the proposed fault diagnosis approach. This dataset collects vibration signals from SKF6205 bearings (SKF Group, Gothenburg, Sweden) using accelerometers at a sampling frequency of 12 kHz. It includes four load conditions: 0 hp, 1 hp, 2 hp, and 3 hp, corresponding to motor speeds set at 1797 r/min, 1772 r/min, 1750 r/min, and 1730 r/min, respectively. The four bearing states adopted in the experiment are categorized as: Normal Class (NC), Inner Race Fault (IF), Outer Race Fault (OF), and Rolling Element Fault (RF).
The fault diameters are further divided into 7 mils, 14 mils, and 21 mils, resulting in a total of 9 fault types. Example vibration signals corresponding to these states are shown in Fig. 3. Additionally, to enhance model robustness, 10dB white noise is randomly added to the original vibration signals during model training to improve the model's noise immunity.
To measure model accuracy, precision, recall, and F1-score are used for evaluation. The relevant calculation formulas are given by Eqs. (22-24).

$$P = \frac{TP}{TP+FP} \quad (22)$$

$$R = \frac{TP}{TP+FN} \quad (23)$$

$$F1 = \frac{2}{1/P+1/R} \quad (24)$$

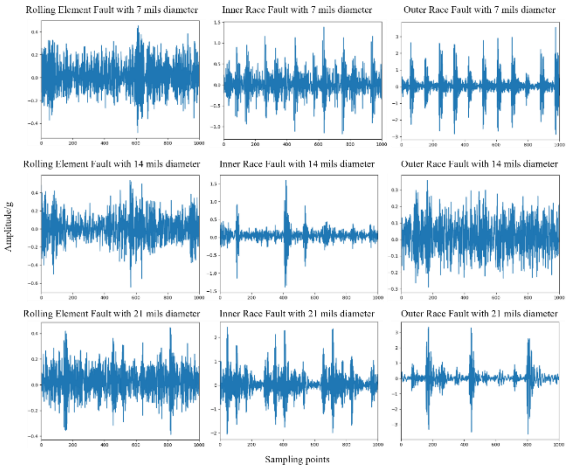

Fig. 2. Examples of vibration signals for 9 different fault types.

In Eqs. (22-24), TP (True Positive) represents the number of positive samples correctly predicted; FP (False Positive) represents the number of negative samples incorrectly predicted as positive; FN (False Negative) represents the number of positive samples incorrectly predicted as negative.

4.2. Data splitting

The calculation formulas for the outer race fault frequency, inner race fault frequency, and rolling element fault frequency are given by Eqs. (25-27), respectively:

$$f_o = 0.5 \times z \times f \times \left(1 - {}^{d}/_{D}\, cos\alpha\right) \quad (25)$$

$$f_i = 0.5 \times z \times f \times \left(1 + {}^{d}/_{D}\, cos\alpha\right) \quad (26)$$

$$f_r = {}^{D}/_{d} \times f \times \left(1 - \left({}^{d}/_{D}\right)^{2} cos^{2}\alpha\right) \quad (27)$$

In the equations, d represents the rolling element diameter, D represents the pitch diameter, α represents the bearing contact angle, and z represents the number of rolling elements. For the SKF6205 bearing used in the CWRU dataset, $f\_o \approx 104HZ$, $f\_i \approx 158HZ$, $f\_r \approx 13.4HZ$. To capture periodic impacts, the minimum sampling window must contain at least 3 complete fault cycles. Therefore, the minimum window size is: $3/\min(f\_o, f\_i, f\_r) \approx 224ms$

Secondly, to avoid data leakage caused by window overlap, the sample segmentation strategy employed in this experiment uses fixed-length overlapping framing. Specific steps are detailed in Table 1.

Finally, the dataset partitioning strategy is shown in Fig. 4. Additionally, reproducibility is ensured by setting a random seed to "1234".

Table 1. Sample partitioning procedure.

Input: signal, window_size, overlap_ratio
Segments = [ ] s = floor(window_size × (1 − overlap_ratio)) for start from 0 to len(signal) − $\text{window}_{\text{size}}$; step = s: segment = signal[start: start + window_size] egments. append(segment)
Output:segments

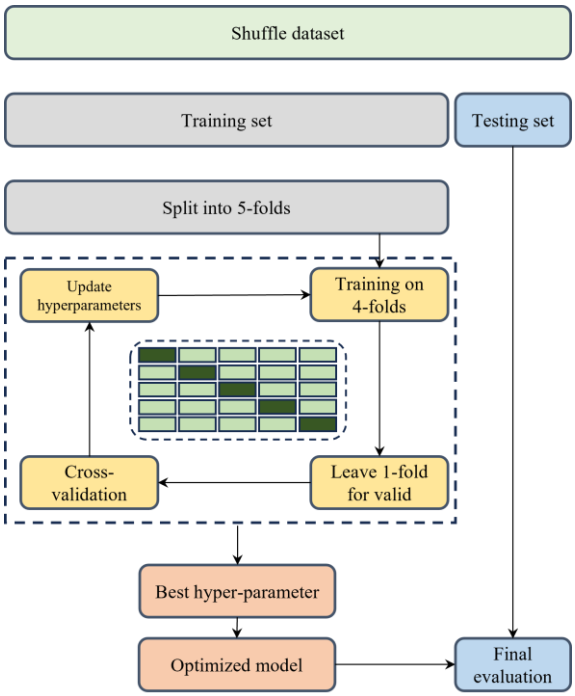

Fig. 3. Dataset partitioning scheme.

4.3. Experimental environment and parameter setting

Regarding experimental software and hardware, the Python version used is 3.10.12, Scikit-learn version is 1.3.0, NumPy version is 1.24.3, and the random seed for dataset splitting is set to 1234. At the sample segmentation level, the fixed-length overlapping framing method is adopted, with a window size of 4000 points and a step size of 2800 points.

For hyperparameter tuning at the model level, a grid search method is employed for optimization. The optimal combination is selected based on 5-fold cross-validation from the search ranges. After PCA dimensionality reduction, the 102-dimensional features are reduced to 4±0 dimensions (cumulative variance of 99.3%). The optimal value for the regularization parameter "C" is 55; the optimal value for the RBF kernel parameter "γ" is 0.05.

The search range for the regularization parameter "C" was: {0.01, 0.1, 1, 10, 45, 55, 100, 300, 500}. The search range for the RBF kernel parameter "γ" was: {0.01, 0.05, 0.1, 0.5, 1, 5}. The F1-score served as the selection criterion for the 5-fold cross-validation.

Hyperparameter selection at the time-frequency feature processing level was determined through subsequent comparative experiments. The final hyperparameters chosen are: using the "db3" wavelet basis for 3-level decomposition and soft thresholding denoising.

4.4. Test set experiments results

The confusion matrix of the proposed method on the final test set is shown in Fig. 5. The prediction performance for each fault type is detailed in Table 2. Overall, Precision is 97.0%, Recall is 96.9%, and the F1-score is 96.9%. Regarding detection accuracy, the proposed method does not advance beyond deep learning-based paradigms (which typically exceed 99% accuracy).

However, this work adopts a traditional feature engineering + SVM approach, offering advantages over deep learning in lower memory consumption, reduced computational complexity, and simplified edge deployment—aligning better with practical industrial requirements.

Using only frequency-domain features from the drive-end vibration signal as input with an SVM classifier (baseline model), the confusion matrix on the test set is shown in Fig. 6. The baseline model achieves 94.1% Precision, 93.9% Recall, and a 94.0% F1-score.

In summary, addressing practical production needs, the proposed model improves upon the feature-engineering baseline (Precision: 94.1% → 97.0%; Recall: 93.9% → 96.9%; F1-score: 94.0% → 96.9%). While its accuracy lags behind deep learning, its low memory footprint (12KB), minimal computational overhead (0.6ms inference), and ease of edge deployment retain significant practical value.

Table 2. Per-class fault prediction report.

Fault Category	Precision (%)	Recall (%)	F1-score (%)	Support
Rolling element fault with 7 mils diameter	92.4	97.3	94.8	75
Rolling element fault with 14 mils diameter	93.1	89.3	91.2	75
Rolling element fault with 21 mils diameter	95.8	90.1	93.1	75
Inner race fault with 7 mils diameter	98.7	100.0	99.3	75
Inner race fault with 14 mils diameter	100.0	100.0	100.0	75
Inner race fault with 21 mils diameter	98.7	100.0	99.3	75
Outer race fault with 7 mils diameter	100.0	97.3	98.6	75
Outer race fault with 14 mils diameter	100.0	100.0	100.0	75
Outer race fault with 21 mils diameter	93.5	96.0	94.7	75
Normal	97.4	98.7	98.0	75

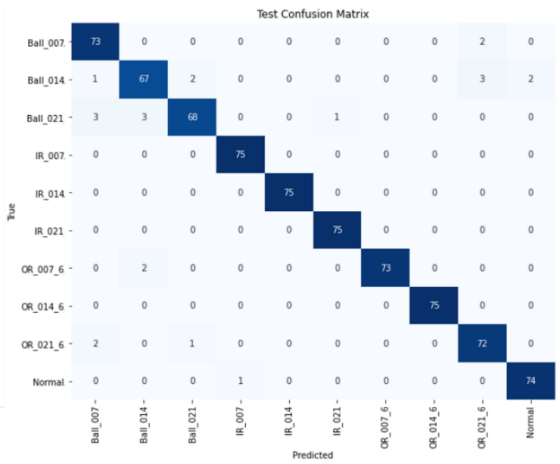

Fig. 4. Confusion matrix of the proposed pipeline on the test set.

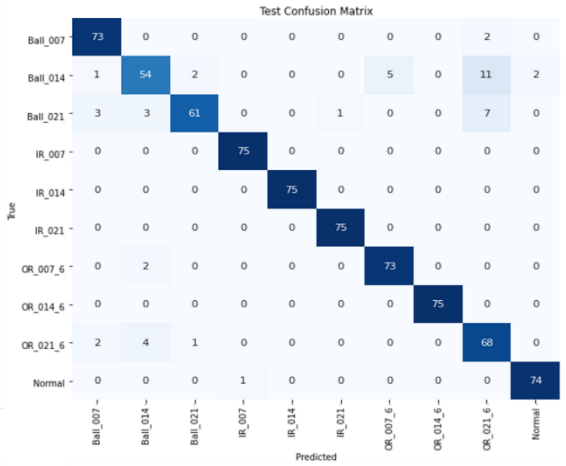

Fig. 5. Confusion matrix of the baseline on the test set.

4.5. Comparative experiments and ablation studies

This section investigates the impact of wavelet packet decomposition hyperparameters. Wavelet decomposition serves dual purposes: extracting frequency-domain features and denoising vibration signals via thresholding before reconstructing time-domain statistics. Wavelet basis and decomposition level require balancing denoising efficacy and feature extraction.

①Denoising Perspective: 3-level decomposition offers optimal cost-effectiveness. Table 3 compares denoising performance (under 10dB added white noise) across wavelet bases and decomposition levels. Algorithm complexity grows exponentially with decomposition depth. For real-time processing on microcontrollers, levels 3 or 4 are practical. Table 3 shows significant denoising improvement from level 2 to 3 across all bases, while level 4 offers marginal gains at double the computation. Thus, a 3-level decomposition is selected.

②Feature Extraction Perspective: As shown in Table 4, the proposed method achieves a lower F1-score than CNN-based approaches but outperforms traditional nonlinear classifiers, while its inference time and model size remain suitable for industrial applications. Furthermore, ablation studies in Table 5 demonstrate that the combination of "db3" with 3-level decomposition and soft thresholding achieves an optimal balance between algorithmic scale and detection accuracy. These findings are consistent with the denoising performance summarized in Table 3, where "db3" and "sym3" were identified as achieving the best denoising performance at 3 decomposition levels.

Table 3. Comparative experiments.

Model	F1-score	Training time	Inference time	Params
Linear SVM	95.2%	11s	0.2ms	12KB
Proposed method	96.9%	12s	0.6ms	12KB
Random Forest	95.8%	9s	1.1ms	11KB
XGBoost	96.2%	22s	0.9ms	11KB
1D-CNN	99.3%	9mins	4ms	2.1MB

Table 4. Denoising performance comparison.

Wavelet Basis	2-Layer Decomposition		3-Layer Decomposition		4-Layer Decomposition	
	Soft Threshold	Hard Threshold	Soft Threshold	Hard Threshold	Soft Threshold	Hard Threshold
db2	17.3	17.3	19.4	19.4	21.0	21.0
db3	17.4	17.4	20.0	20.0	21.7	21.8
db4	17.4	17.4	19.8	19.9	21.1	21.2
db5	17.3	17.4	19.8	19.8	21.8	21.9
db10	17.3	17.3	19.8	19.9	20.9	20.9
haar	17.3	17.4	19.2	19.2	18.3	18.3
sym2	17.3	17.3	19.4	19.4	21.0	21.0
sym3	17.3	17.3	19.9	20.0	21.7	21.8
sym4	17.3	17.3	19.9	19.9	21.5	21.5
sym5	17.3	17.3	19.8	19.8	21.8	21.8
sym6	17.3	17.3	19.8	19.8	21.3	21.3
coif1	17.3	17.3	19.9	19.9	21.9	21.9
coif2	17.3	17.3	19.7	19.7	21.1	21.1
coif3	17.3	17.3	19.9	19.9	20.8	20.7
bior1.1	17.4	17.4	19.2	19.2	18.3	18.3
bior2.4	17.2	17.2	19.7	19.7	21.6	21.6
bior3.3	16.5	16.5	18.4	18.0	19.0	18.9
rbio1.1	17.4	17.4	19.2	19.2	18.3	18.3
rbio2.4	17.3	17.3	19.8	19.8	21.6	21.6
rbio3.3	16.6	16.6	18.4	18.4	17.8	17.8
rbio4.4	17.3	17.3	19.8	19.8	21.5	21.5
dmey	17.3	17.3	19.9	19.9	21.2	21.6

Table 5. Ablation study.

Wavelet basis	Dimless stats	Multi-Src signals	Denoising	PCA	SVM	Params	P	R	F1
×	×	×	×	×	√	1.5MB	94.1%	93.9%	94.0%
sym3	√	×	×	×	√	1.1MB	95.0%	94.9%	94.9%
sym3	√	√	×	×	√	1.5MB	96.2%	97.0%	96.6%
sym3	√	×	√	×	√	1.1MB	95.3%	95.4%	95.3%
sym3	×	×	√	×	√	1.1MB	94.8%	95.1%	94.9%
sym3	√	√	√	×	√	1.5MB	97.4%	97.2%	97.3%
sym3	√	√	√	√	√	12KB	96.5%	96.7%	96.6%
db3	√	×	×	×	√	1.1MB	95.2%	95.0%	95.1%
db3	√	√	×	×	√	1.5MB	96.8%	97.1%	96.9%
db3	√	×	√	×	√	1.1MB	95.5%	95.6%	95.5%
db3	×	×	√	×	√	1.1MB	95.1%	95.2%	95.1%
db3	√	√	√	×	√	1.5MB	97.8%	97.4%	97.6%
db3	√	√	√	√	√	12KB	97.0%	96.9%	96.9%

5. Conclusions

This study proposes an embedded intelligent detection framework for rolling bearing fault diagnosis, achieving an effective balance among detection accuracy, computational efficiency, and noise robustness. The core innovations and findings are as follows:

① Multi-source signal fusion anti-noise mechanism. By synchronously acquiring vibration signals from the drive end and fan end along with their differential signal to construct three-channel inputs, and employing wavelet decomposition-based hard threshold denoising, 20.0 dB noise suppression is achieved under strong 10 dB noise conditions, significantly enhancing the model's noise immunity.

② Cross-condition time-frequency domain feature engineering. The introduction of frequency-domain features (e.g., unit node energy entropy and wavelet coefficient standard deviation) combined with rotation-invariant dimensionless indicators (kurtosis factor/waveform factor/impulse factor) effectively strengthens time-domain characterization and improves model generalizability.

③ Model lightweighting. By incorporating PCA for feature dimensionality reduction between feature extraction and classifier prediction, the proposed model further reduces computational demands. The overall model size is only 12 KB (1/175 of a CNN model), inference latency is 0.6 ms (1/7 of a CNN model), and the F1-score reaches 96.9% (2.4% lower than CNN), enabling direct deployment on battery-powered edge devices.

④ Performance validation. Under identical 10 dB noise environments, the proposed method demonstrates a 2.9% precision increase and a 3.0% recall improvement compared to the baseline model.

In summary, this research provides a bearing fault diagnosis solution deployable directly on low-power embedded edge computing platforms. Future work will explore lightweight detection methods based on deep learning paradigms to further deliver high-precision, low-cost embedded solutions for rotating machinery fault diagnosis.

Acknowledgment

This research was funded by Open Foundation of Industrial Perception and Intelligent Manufacturing Equipment Engineering Research Center of Jiangsu Province (Grant No. ZK22-05-01), and Start-up Fund for New Talented Researchers of Nanjing Vocational University of Industry Technology (Grant No. YK23-01-01).

References

[1] A. Rai and S. H. Upadhyay, "A review on signal processing techniques utilized in the fault diagNosis of rolling element bearings," *Tribol. Int.*, Vol. 96, pp. 289-306, (2016).

[2] B. Wang, Y. Lei, N. Li, and N. Li, "A Hybrid ProgNostics Approach for Estimating Remaining Useful Life of Rolling Element Bearings," *Ieee. T. Reliab.*, Vol. 69, No. 1, pp. 401-412, (2020).

[3] S. Qiu, h. Zhao, N. Jiang, Z. Wang, L. Liu, Y. An, H. Zhao, X. Miao, R. Liu and G. Fortino, "Multi-sensor information fusion based on machine learning for real applications in human activity recognition: State-of-the-art and research challenges," *Inform. Fusion.*, Vol. 80, pp. 241-265, (2022).

[4] L. H. Wang, X. P. Zhao, J. X. Wu, Y. Y. Xie, and Y. H. Zhang, "Motor Fault DiagNosis Based on Short-time Fourier Transform and ConVolutional Neural Network," *Chin. J. Mech. Eng-En.*, Vol. 30, No. 6, pp. 1357-1368, (2017).

[5] O. Abdeljaber, S. Sassi, O. Avci, S. Kiranyaz, A. A. Ibrahim, and M. Gabbouj, "Fault Detection and Severity Identification of Ball Bearings by Online Condition Monitoring," *Ieee. T. Ind. Electron.*, Vol. 66, No. 10, pp. 8136-8147, (2019).

[6] A. A. Ballakur and A. Arya, "Empirical Evaluation of Gated Recurrent Neural Network Architectures in Aviation Delay Prediction," *ICCCS*, pp. 1-7, (2020).

[7] S. Hochreiter and J. Schmidhuber, "Long Short-Term Memory," *Neural. Comput.*, Vol. 9, No. 8, pp. 1735-1780, (1997).

[8] A. Vaswani et al., "Attention is All you Need," *Neural. IPS.*, (2017) .

[9] C. Chen, Y. Yuan, and F. Zhao, "Intelligent Compound Fault DiagNosis of Roller Bearings Based on Deep Graph ConVolutional Network," *Sensors*, Vol. 23, No. 20, pp. 8489, (2023).

[10] Z. Wang, Y. Dong, W. Liu, and Z. Ma, "A Novel Fault DiagNosis Approach for Chillers Based on 1-D ConVolutional Neural Network and Gated Recurrent Unit," *Sensors*, Vol. 20, No. 9, pp. 2458, (2020).

[11] X. Li, Y. Yang, H. Y. Pan, J. Cheng, and J. S. Cheng, "A Novel deep stacking least squares support vector machine for rolling bearing fault diagNosis," *Comput. Ind.*, Vol. 110, pp. 36-47, (2019).

[12] Y. Shao, X. F. Yuan, C. J. Zhang, C. Z. Liu, and Ieee, "Rolling Bearing Fault DiagNosis Based on Wavelet Package Transform and IPSO Optimized SVM," *CCDC*, pp. 2758-2763, (2020)

[13] G. Li, C. Deng, J. Wu, Z. Chen, and X. Xu, "Rolling Bearing Fault DiagNosis Based on Wavelet Packet Transform and ConVolutional Neural Network," *Appl. Sci-Basel.*, Vol. 10, No. 3, pp. 770, (2020).

[14] Y. K. Sun, Y. Cao, G. Xie, and T. Wen, "Sound Based Fault DiagNosis for RPMs Based on Multi-Scale Fractional Permutation Entropy and Two-Scale Algorithm," *Ieee. T. Veh. Technol.*, Vol. 70, No. 11, pp. 11184-11192, (2021).

[15] Y. Q. Wu, J. Dai, X. Yang, F. Shao, J. Gong, P. zhang and S. Liu, "The Fault DiagNosis of Rolling Bearings Based on FFT-SE-TCN-SVM," *Actuators*, Vol. 14, No. 3, (2025).

[16] J. L. Song, Z. Y. Shi, B. H. Du, L. Y. Han, H. G. Wang, and Z. W. Wang, "MEMS gyroscope wavelet de-Noising method based on redundancy and sparse representation," *Microelectron. Eng.*, Vol. 217, (2019).

[17] S. Ehrich, "On the estimation of wavelet coefficients," *Adv. Comput. Math.*, Vol. 13, No. 2, pp. 105-129, (2000).

[18] J. Roffers-Agarwal, K. J. Hutt, and L. S. Gammill, "Paladin is an antiphosphatase that regulates neural crest cell formation and migration," *Dev. Biol.*, Vol. 371, No. 2, pp. 180-190, (2012).

[19] L. Ouahid, H. Nebdi, and L. Dalil-Essakali, "Kurtosis factor of truncated and Non-truncated simplified general-type beams," *Opt. Quant. Electron.*, Vol. 49, No. 3, (2017).

[20] L. S. Kwon and L. E. E. Jaemin, "A Study on the Structural Causal Relationship of Marketing Stimulating Factors on Online Impulse Purchase through Consumer Value : Focusing on the Mediating Effect of Consumer Value," *J. Wellbeing Manag. Appl. Psychol.*, Vol. 5, No. 3, pp. 7-17, (2022).

[21] C. Casari, P. J. Lenting, N. Wohner, O. D. Christophe, and C. V. Denis, "Clearance of von Willebrand factor," *J. Thromb. Haemost.*, Vol. 11, pp. 202-211, (2013).

[22] W. A. Smith and R. B. Randall, "Rolling element bearing diagNostics using the Case Western Reserve University data: A benchmark study," *Mech. Syst. Signal. Pr.*, Vol. 64-65, pp. 100-131, (2015).

How to cite this paper:

A. Haitao Zhang, B. Li Guan and C. Long Chang, " A vibration-based fault diagnosis method for rolling bearings via optimized wavelet-SVM fusion", *J. Comput. Appl. Res. Mech. Eng.*, Vol. 15, No. 1, pp. 63-74, (2025).

DOI: 10.22061/jcarme.2025.10582.2401

URL: https://jcarme.sru.ac.ir/?_action=showPDF&article=2410